



Journal of Advanced Research in Fluid Mechanics and Thermal Sciences

Journal homepage:
https://semarakilmu.com.my/journals/index.php/fluid_mechanics_thermal_sciences/index
ISSN: 2289-7879



Multi-Objective Optimization of Vortex Magnetohydrodynamics (MHD) Generator using Response Surface Methodology

Arleen Natalie¹, Ridho Irwansyah^{1,*}, Budiarmo¹, Nasruddin¹

¹ Department of Mechanical Engineering, Faculty of Engineering, Universitas Indonesia, 16424 Depok, Indonesia

ARTICLE INFO

Article history:

Received 4 November 2023

Received in revised form 22 February 2024

Accepted 5 March 2024

Available online 30 March 2024

Keywords:

Magnetohydrodynamics; MHD generator; multi-objective optimization; Response Surface Methodology

ABSTRACT

The introduction of electromagnetic fields in fluid dynamics in magnetohydrodynamics (MHD), particularly when those fields are vector and non-uniform, complicates its application in vortex geometry. The imperative to optimize MHD generators arises from the inherent trade-off between voltage and pressure drop in energy conversion systems, to maximize voltage output while minimizing associated pressure drop. This study focuses on optimizing vortex MHD generators by applying Response Surface Methodology (RSM), which is based on mathematical models that capture the complex relationships between factor and response variables. This method offers a comprehensive approach to obtaining the optimum solution to the objectives, voltage and pressure drop, based on fluid velocity and magnetic field strength input parameters. Numerical optimization RSM generates 11 solutions. The optimum solutions obtained are a velocity of 1.415 m/s, and magnetic field strength of 0.43 T, and the corresponding optimum output voltage and pressure drop will be 4.264 mV and 4.254 psi, respectively, with a desirability level of the selected solution is 0.770. This study suggests the RSM method shows a good measurement of R^2 and RSME. Our findings contribute to the understanding of optimizing vortex MHD generators and offer insights into achieving efficient energy conversion systems of a set of optimum generator operating parameters.

1. Introduction

It is evident that the need for clean and sustainable energy sources is increasing substantially as the impacts of climate change become more apparent. As a result, interest in alternative energy sources that are clean, renewable, and efficient is growing. In conventional hydropower generation, primary energy in the form of fluid flows into the turbine, rotating the shaft in the generator as mechanical energy. For the second time, it is converted into electrical energy through electromagnetic induction. This repetitive conversion process results in an energy loss of approximately 65% before being distributed to the end user. Integrating a direct conversion system has proven beneficial to power generation systems. According to a study conducted by Sheikholeslami *et al.*, when a thermoelectric generator (TEG) installed at the back of a photovoltaic

* Corresponding author.

E-mail address: ridho.irwansyah@ui.ac.id

<https://doi.org/10.37934/arfmts.115.2.3349>

(PV) panel can efficiently use waste heat to increase electrical production and electrical efficiency according to [1] and even though there may be possible drops in PV efficiency at high irradiation levels, increased temperature differentials amongst TEG modules boost electricity generation and improve the unit's thermal efficiency (η_{th}) [2]. The study focuses on the direct conversion of fluid to electricity, a Magnetohydrodynamics (MHD) generator that converts the mechanical energy of an electrically conducting flowing fluid directly into electricity using a magnetic field. Because MHD generators remove the intermediate step of the prime mover, it has no mechanically moving parts. Hence, their designs are simpler and more portable than conventional generators.

Earlier development of MHD generator using simple chamber geometry as a channel for conducting fluid to flows, such as vertical duct [1-4], horizontal duct [3,5-9] horizontal with reciprocating system to produce alternating current (AC) experimented by Domínguez-Lozoya *et al.*, [8,10] and cylindrical annular geometry theoretically studied by Pérez-Orozco J.A. and Ávalos-Zúñiga R. A. [9,11]. The most significant energy loss in this type of channel occurs due to end effects caused by the magnetic field's non-homogeneity and the electrodes' finite length [8,10-12]. This can be solved by creating a vortex chamber that maximizes its power production in such a compact shape. Nowadays, researchers are focusing a study on vortex-type MHD generators [11-17]. The reference used for this study, Panchadar *et al.*, [13,15] conduct the circular swirling flow that forms in the circular vortex MHD generator is confirmed to be capable of producing electrical energy with a potential power density of 34 W/cm^3 , with optimization allowing for a power density of approximately 10^2 W/cm^3 . Both theoretical and experimental investigations confirm this.

Generally, these findings show the relation between parameters and performance output in the MHD generator. Takeda *et al.*, [1,3] performed a comprehensive experimental study on a helical-type MHD generator, concluding that electromotive force rose linearly with increasing average flow velocity in a constant magnetic field. Another finding is that the generator output increased quadratically to average flow velocity and magnetic field over specific points. As observed by Kobayashi, Shionoya, and Okuno [3,5], as the magnetic flux density (or Hartmann number) increases, the eddy current becomes greater, increasing the forces opposing the flow. The same effect is noticed in Lorentz force [2,4,6]. Electric power increases as Hartmann (Ha) number values increase, but this does not occur when substantial values of Ha number are reached through a simulation study performed by Cosoroaba *et al.*, [4,6]. The relationship between oscillation frequency and voltage, whereas current is found to rise almost linearly, observed by Domínguez-Lozoya *et al.*, [8,10]. Gupta, Taylor, and Krupenkin [14,16] found that a MHD generator using a rotating impeller is able to generate up to 3 W of power and shows an optimum point of power produced at a current of 6 A due to a saturation limit of the material. Another form of loss is the loss due to Joule heating [9,16] [7,14]. The investigation of a non-Newtonian Reiner-Rivlin fluid reveals that higher Reynolds numbers generally lead to increased velocities and lower temperature distributions in two infinitely revolving disks [18] and shows that an increase in the magnetic parameter corresponds to higher average axial and radial velocities, but a decrease in the average transverse velocity and temperature profile in two plates, conducted by Jalili *et al.*, [19].

The study of optimization has grown in popularity in recent years due to its widespread applications in various fields. The growing optimization study emphasis on sustainability and environmental concerns has led to optimization being employed to address resource allocation and energy efficiency challenges. The multi-objectives optimization problem addresses the complexity of today's issue. Response Surface Methodology (RSM) and Artificial Neural Network (ANN) are the most common optimization methods. A significant collection of training data is typically needed for ANN optimization to effectively capture complicated patterns and generalize. The greater sample size contributes to better generalization performance and less overfitting. Conversely, RSM can

occasionally function with smaller sample numbers, particularly when the experiment design is properly planned out to capture the relevant information effectively [20]. RSM's optimization mathematical model is established between the target and the impact factor, which can determine the optimal variable parameters, as stated by Zhu *et al.*, [17,21]. This method has been widely used to solve problems with conflicting factors in various applications. Sunarti *et al.*, [22] used RSM to optimize the performance of the automated control system of Membrane Gas Absorption utilizing the manufactured thin film composite (TFC) with a difference of no more than 5% between the actual and predicted data. In one study proposed by Deshmukh *et al.*, [23] to maximize the fundamental frequency of e-glass epoxy composite panels with four input parameters (aspect ratio, thickness ratio, number of plies, and ply angle), the RSM method has been used to create a second order equation that describes the intended response, with a result of desirability of the study is 0.89. The effectiveness of the optimization method, which significantly decreases the optimization cost and produces valuable results, has been demonstrated by Kong *et al.*, [18,24]. In power generation devices, researchers [19-22,25-28] proved that the practical implementation of RSM could enhance the performance of objectives compared to those reported in the literature. Another study that benefits from RSM optimization was established to design a small-scale wind power generator performed by Lee *et al.*, [23,29]. The inefficiency of the cogging torque was reduced by 92.6% from the initial model, and the total harmonic distribution of the back electromotive force that causes the prevailing power source was reduced by 75.2%.

Two publications related to the optimization of MHD generators have been reported. Ibanez, Cuevas, and Haro [24,30] reported an optimization study for an alternate MHD generator, resulting in a maximum electrical isotropic efficiency of 66%, with values of parameters such as load factor, Hartmann number, and oscillation Reynolds number of 0.5, 450, 1.37×10^6 , respectively. The obtained optimum value is observed analytically with no particular optimization process used. Carcangiu, Fanni, and Montisci [16,31] suggested the assessment of a collection of Pareto optimal solutions for an inductive MHD generator by implementing a multi-objective search algorithm based on the Tabu Search metaheuristics (MO-TS) method with three conflicting objectives: maximizing power output, minimizing losses, and minimizing the mass of the device. It is stated that this optimization aims to produce the Pareto Front subdomain of non-dominated solutions rather than to identify the optimal solution. The result suggests a power output of 55.9 kW, the losses amount to roughly 11% of the power output with high-speed gas (400 m/s). The method is already suitable, but the application between induction MHD generators has different parameters.

The advantage of vortex geometry is that it could convert energy more efficiently than other geometries due to no edge losses. Adding electromagnetic fields to fluid dynamics complicates, particularly when the fields are vector and non-uniform. When these fields are employed in vortex geometry, difficulties arise. An analytical approach is needed to determine its optimum parameter because of the complex interactions of the parameters. Hence, specific optimization techniques must be performed. There needs to be more DC current vortex MHD generator optimization studies to address the multi-objective problems. This is confirmed by both theoretical and experimental investigations conducted by Panchadar *et al.*, [13,15]. A counterintuitive phenomenon is shown in both experimental and analytical results, wherein lower pressure drops at the same injection velocity are caused by a decrease in the stated pressure drop as magnetic fields increase, while voltage had the opposite effect. This demonstrates how factors must be traded off to reach optimum goals. The primary field affecting the objective is the velocity field and magnetic field. Aiming to increase the energy density by maximizing voltage and minimizing pressure drop, the goal is to obtain the optimal value of these primary fields, proving the ability of the MHD generator as an efficient power generation available for commercial use. Given the constraints of a small dataset, the utilization of

RSM is particularly suitable in this context, providing a robust and statistically sound optimization approach tailored to the limitations posed by the limited dataset in the analysis of the vortex MHD generator. This study determined to apply the RSM method to attain optimum output based on the report of Panchadar *et al.*, [13,15], and the main contributions of this study primarily revolve around the exploration and optimization of operational conditions and parameters to attain optimal objectives.

2. Methodology

2.1 Materials

MHD generator consists of a pair of magnets, a disc magnet, and a ring magnet, with a coaxial cylindrical chamber in between, as shown in Figure 1. The conducting fluid flows through the chamber from the inlet, rotates tangentially, and then leaves the chamber through the exhaust outlet. The generated current is then collected through the electrode, peripheral electrode, and centre electrode.

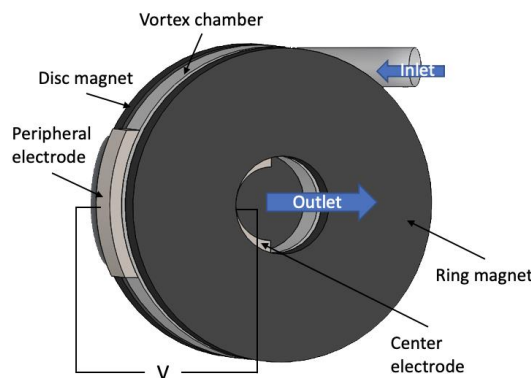


Fig. 1. Vortex MHD generator schematic and components with a front view

The geometry significantly impacts the performance of fluid and field behaviour, as described in Figure 2(a). Three main fields are visualized in Figure 2(b) as follows. The magnetic field is in the direction from top to bottom, perpendicular to conducting fluid that flows towards readers, and the generated current is from the centre to the peripheral electrode, all per Fleming's right-hand rule. The geometry is determined by the chamber's height, the diameter of the inlet and outlet, the inner and outer cylinders, and their respective radii.

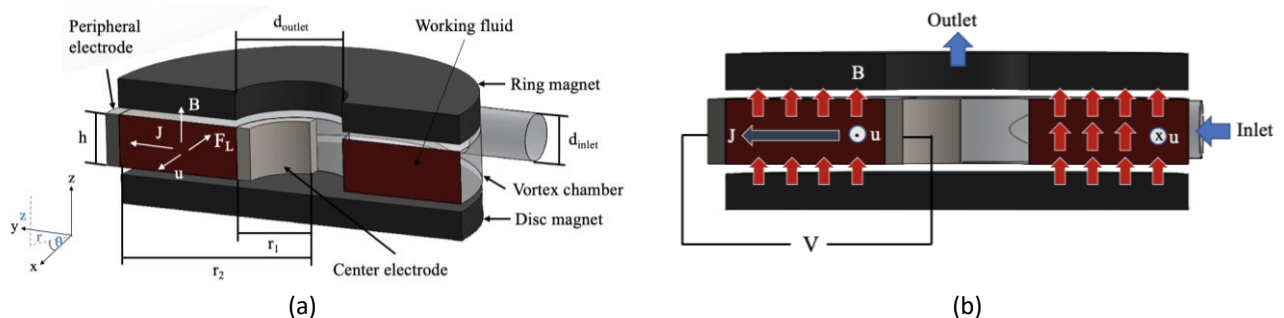


Fig. 2. Geometric parameters of (a) an isometric-side view with geometric parameters and (b) a side-view of velocity, electric, and magnetic field direction

The data in this study is based on the experimental investigation by Panchadar *et al.*, [13,15], and consists of nine data points using variation factors of magnetic field strength and conducting fluid velocity as input, whereas voltage and pressure drop as output that will be optimized later, using mercury (Hg) liquid metal as working fluid. The secondary data were initially in the form of a graph and were then digitized using OriginPro software to obtain their numerical value, as shown in Table 1. Factor 1, fluid velocity, and Factor 2, magnetic field strength, have three levels: 1.23, 1.43, and 1.63 m/s and 0.19, 0.35, and 0.43 T, respectively. The measured output as a response to the experimental study is based on the input factors of voltage and pressure drop with a range of 1.78 to 4.96 mV and 3.39 to 8.98 psi.

Table 1
 Experimental data of vortex MHD generator by Panchadar *et al.*, [13]

No.	Factors		Responses	
	A: Velocity (m/s)	B: Magnetic field strength (T)	R ₁ : Voltage (mV)	R ₂ : Pressure drop (psi)
1	1.23	0.19	1.78	4.78
2	1.43	0.19	2.08	6.98
3	1.63	0.19	2.47	8.98
4	1.23	0.35	3.07	3.58
5	1.43	0.35	3.80	5.27
6	1.63	0.35	4.27	6.78
7	1.23	0.43	3.71	3.39
8	1.43	0.43	4.57	4.90
9	1.63	0.43	4.96	5.87

2.2 Formulation of the Problem

The magnetic and electric fields are governed by a set of equations known as Maxwell's equations, whereas the fluid dynamics is governed by the Navier-Stokes equation. Fluid flow equations comprise one vector and one scalar equation, while Maxwell's equations consist of two vector and two scalar equations. Though fluid mechanics equations are typically nonlinear, Maxwell's equations are usually linear. Therefore, there is still the possibility of addressing issues when Maxwell's equations are introduced. Equations are described in Eq. (1) to Eq. (4) for (i) Maxwell's equations

$$\nabla \times \vec{E} = \frac{\partial \vec{B}}{\partial t}, \quad (1)$$

$$\nabla \times \vec{B} = \mu \vec{J}, \quad (2)$$

$$\nabla \cdot \vec{B} = 0, \quad (3)$$

$$\nabla \cdot \vec{E} = 0, \quad (4)$$

where \vec{E} is electric field, \vec{B} is magnetic field, t is time, μ is magnetic permeability, \vec{J} is current density, and \vec{u} is conducting fluid velocity. Fluid dynamics behaviour are governed by the (ii) continuity equation,

$$\nabla \cdot \vec{u} = 0, \quad (5)$$

and (iii) Navier-Stokes equation,

$$\frac{\partial \vec{u}}{\partial t} + (\vec{u} \cdot \nabla) \vec{u} = -\frac{1}{\rho} \nabla \vec{p} + \nu \nabla^2 \vec{u} + \frac{1}{\rho} (\vec{J} \times \vec{B}) \quad (6)$$

where ρ is fluid density, \vec{p} is pressure and ν is the kinematic viscosity. There are additional forces into Navier-Stokes equations by Lorentz Force $\vec{J} \times \vec{B}$. Through Ohm's law, current density is described by

$$\vec{J} = \sigma (\vec{E} + \vec{u} \times \vec{B}) \quad (7)$$

where σ is electrical conductivity.

The relation of the input parameter to the response can be described in Eq. (8) for voltage or electromotive force V , Eq. (9) for pressure drop between inlet and outlet Δp , and Eq. (10) for characteristic velocity β , as derived by Panchadar *et al.*, [13,15]:

$$V = Bau_2 \cdot \frac{1}{1 + \frac{\beta}{u_2}} \quad (8)$$

$$\Delta p = \frac{\rho \beta^2}{2} \left(\frac{u_2}{\beta} \right)^2 \left[1 + k \left(\frac{u_2}{\beta} \right)^2 \right] \quad (9)$$

$$\beta = \frac{a_2 B^2}{2 \rho S R_t} \cdot \frac{1}{2} \left(1 + \frac{r_2}{r_1} \right) \quad (10)$$

where r_2 is outer radius, r_1 is inner radius, channel width $a = r_2 - r_1$, u_2 is velocity at outer radius, k is minor loss coefficient, S is inlet cross-sectional area, and R_t is total circuit resistance.

The objective of optimization is to maximize voltage while minimizing pressure drop. Maximizing voltage leads to higher power output while minimizing pressure drop can reduce losses, hence leading to higher efficiency. The increased voltage shows two conflicting multi-objectives that the pressure drop will increase. Even though the goal of maximizing voltage is accomplished, trading off the goal of decreasing pressure drop conflicts to minimize it.

Eq. (11) shows the corresponding objective function R_1 as maximizing voltage and function R_2 minimizing pressure drop, both as a function of variable fluid velocity A and magnetic field strength B . Both main effects A and B are within their input range and are set as constraints in the equation.

$$\begin{aligned} \text{Max } R_1 &= R_1(X_1, X_2) \\ \text{Min } R_2 &= R_2(X_1, X_2) \\ \text{Subject to } &1.23 < X_1 < 1.63 \\ &0.19 < X_2 < 0.43 \end{aligned} \quad (11)$$

2.3 Predictive Modelling and Optimization

RSM is one of the Design of Experiment (DoE) methods to predict and build higher polynomials to model non-linear factor-response relationships [25,32]. It helps researchers understand and optimize complex systems' relationships between input variables (factors) and response variables

(outputs). The main goal of RSM is to find the optimal combination of input variables that will yield the desired or optimum values for the response variables. RSM achieves this by systematically designing and conducting experiments, collecting data, and constructing mathematical models to represent the relationship between the variables.

RSM employs carefully designed experiments, often using factorial or fractional factorial designs, to explore the effects of various input variables on the response variables. These experiments are conducted to collect data on the response variables at different levels of the input variables. The collected data is then used to develop mathematical models describing the relationship between the input and response variables. RSM commonly employs second-order polynomial models, capturing the input variables' linear and quadratic effects. Regression analysis based on the mathematical model of the data, two-factor interaction, can be formulated as Eq. (12) stated by Naveen *et al.*, [26,33]

$$R_{i(2FI)} = b_0 + b_1 X_1 + b_2 X_2 + b_3 X_1 X_2 \quad (12)$$

where $R_{i(2FI)}$ is the response variable, b_0 is the arithmetic means of the response of all trials, b_i is the estimated coefficient for factor X_i , X_i is the main effect-i, and $X_i X_j$ is the interaction between main effects i and j.

The constructed models are analysed using statistical techniques such as analysis of variance (ANOVA) to assess the significance of the input variables and their interactions. This analysis helps identify the most influential factors and determine their optimal levels for achieving the desired response. Finally, RSM utilizes optimization algorithms, such as the gradient descent method or response surface optimization, to find the optimal settings for the input variables that maximize or minimize the response variables. These algorithms navigate the mathematical models to locate the regions of maximum or minimum response values. Once the optimal settings are determined, the RSM models and results are validated by conducting additional experiments or comparing them with real-world observations. This step ensures the reliability and accuracy of the optimized settings and helps confirm the effectiveness of the RSM approach. Results can be measured in terms of error and differences between the predicted and actual values, using the Root Mean Square of Error from Eq. (13).

$$RMSE = \sqrt{\frac{\sum_{i=1}^n (y - x)^2}{n}} \quad (13)$$

where y is the actual data, x is the predicted data, and n is the number of samples.

Numerical optimization in Design Expert using Response Surface Methodology (RSM) involves the process of finding the optimal combination of input variables or factors that maximizes or minimizes a response or output variable of interest. During the optimization process, the algorithm adjusts the values of the input variables within specified ranges to find the combination that yields the most desirable response. It can use various optimization techniques, such as gradient-based methods or evolutionary algorithms, to navigate the design space and converge towards the optimal solution. The optimization algorithm continues to refine the input variable values until a stopping criterion, such as a maximum number of iterations or a desired level of improvement in the response variables, is met. Once the optimization process is complete, the Design Expert provides the optimal set of input variables that can be used to achieve the desired response. Critical points of RSM utilization summarized by Ray *et al.*, [20,27]:

- i. Model Complexity: RSM uses less complex mathematical models, like polynomial equations, to approximate the relationship between variables.
- ii. Objective Function: By changing the input variables to attain the desired target value or maximum/minimum response, RSM usually seeks to optimize an output variable or response.
- iii. Optimization Algorithms: RSM optimization employs methods based on experiments or least squares regression design to estimate the response surface model's coefficients.
- iv. Training Data and Sample Size: RSM can occasionally work with smaller sample sizes, mainly when experiment designs are carefully considered to capture relevant information effectively.
- v. Assumptions and Limitations: RSM frequently assumes that a polynomial equation can accurately represent the response surface within the given input range.

3. Results

3.1 RSM model

The RSM optimization is carried out using secondary data from Table 1 and the definition of the objective and parameters is given in Eq. (11). Data is imported to DesignExpert v12 software, where custom designs are utilized to perform the modelling due to adjustments to the experiment that cannot be accommodated by the standard design. Secondary data determined the values of both input and response. Historical mode is chosen to design based on an existing data set to perform predictive modelling, then is optimized. The flow of the RSM optimization process is described explicitly in Figure 3.

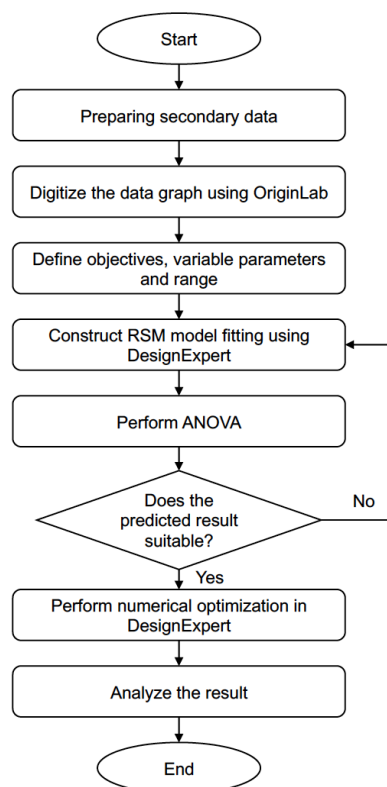


Fig. 3. Flowchart of vortex MHD generator RSM optimization

The fit statistics in Table 2 show a slightly better result measured in R^2 , using the best lambda value based on the Box-Cox Plot, then the study is carried on with lambda for voltage and pressure drop are 1.59 and 0.5, respectively. A higher R^2 implies that a more significant portion of the differences observed in the dependent variable can be accounted for in the independent variable. Adequate precision on both responses in the transformed version also shows a higher value that can be interpreted as higher accuracy in the estimation obtained from a statistical model or analysis. It suggests that the findings are sufficiently precise to draw meaningful conclusions.

Table 2

Fit statistics for voltage and pressure drop

Response	Voltage (R_1)	Pressure drop (R_2)
Std. Dev.	0.1907	0.0365
Mean	7.36	2.34
C.V. %	2.59	1.56
R^2	0.9983	0.9939
Adjusted R^2	0.9972	0.9902
Predicted R^2	0.9943	0.9869
Adeq Precision	82.2397	47.8992

The interaction between Factor A and Factor B is suggested as a two-factor interaction for both responses. ANOVA was then performed to see parameter significance, which shows all parameters and their interactions are significant (p-value < α , where α is 0.05), except for factor AB in pressure drop in Table 3. This implies that the interaction between velocity and magnetic field strength is not significantly related to pressure drop.

Table 3

ANOVA for voltage and pressure drop

Response	Model	Source	Sum of Squares	df	Mean Square	F-value	P-value
R ₁ : Voltage (Power to 1.59)	2 FI	Model	105.22	3	35.07	964.90	< 0.0001
		A: velocity	17.38	1	17.38	478.12	< 0.0001
		B: magnetic field strength	73.36	1	73.36	2018.23	< 0.0001
		AB	3.21	1	3.21	88.27	0.0002
		Residual	0.1817	5	0.0363		
		Cor Total	105.40	8			
R ₂ : Pressure drops (Square root)	2 FI	Model	1.08	3	0.3610	270.92	< 0.0001
		A: velocity	0.7551	1	0.7551	566.62	< 0.0001
		B: magnetic field strength	0.4028	1	0.4028	302.25	< 0.0001
		AB	0.0045	1	0.0045	3.39	0.1248
		Residual	0.0067	5	0.0013		
		Cor Total	1.09	8			

To describe in mathematical form based on Eq. (5), regression equations were obtained in Eq. (14) and Eq. (15).

$$R_1^{1.59} = 6.77 + 1.77A + 3.46B + 0.9222AB \tag{14}$$

$$R_2^{0.5} = 2.34 + 0.3681A - 0.2564B - 0.0346AB \tag{15}$$

where the two responses are voltage (R_1) and pressure drop (R_2), and two factors are velocity (A) and magnetic field strength (B). Variable AB is the interaction of both factors.

The exponent on both functions is a transformation based on the suggested lambda. All variables, including velocity and the strength of the magnetic field as well as their interaction, positively correlate with voltage to the power of 1.59 in Eq. (14). The coefficients of each factor's variables show how significantly they affect the corresponding response. Factor B , magnetic field strength, contributes the most to voltage in a positive direction, followed by velocity and their interaction ($B > A > AB$). For the square of pressure drop in Eq. (15), velocity is the only factor that affects in a positive direction. In contrast, magnetic field strength, followed by interaction between both factors (Factor AB), affects it in the opposite direction. It tells that as magnetic field strength and both factors' interactions increase, it will decrease the value of pressure drop. The significance of the factor's effect is already confirmed by the ANOVA test when the p-value is less than alpha.

If the residuals follow a normal distribution, it can be determined using the normal probability plot (straight line). In Figure 4, the value range for voltage is 2.501–12.759 mV while for pressure drop is 1.841–2.997 psi. There are some data points that deviate from the normal line, which will be validated further in the next diagnosis.

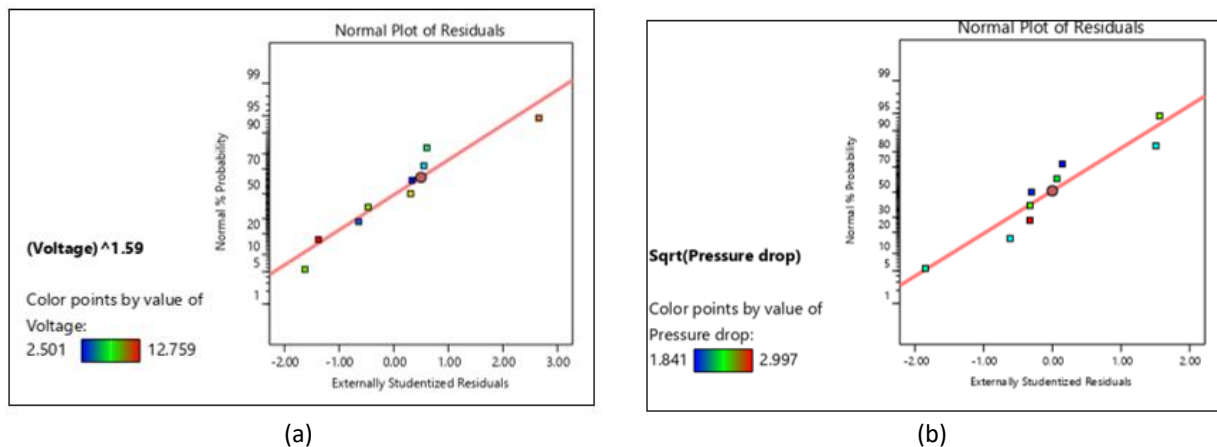


Fig. 4. Normal plot for (a) voltage and (b) pressure drop

The residuals versus predicted response values plot should be a random scatter (constant residual range across the graph). The data points on the graph are randomly distributed. Figure 5 indicates that the residuals versus experimental run-order plot look for hidden variables that may have influenced the response during the experiment. The plot has a tendency of a “<” pattern, while it is supposed to display a random scatter. Blocking and randomization are suggested to protect against trends undermining the analysis. The plot of the residuals versus any factor checks whether the variance not accounted for by the model is different for different levels of a factor. The plot exhibits a random scatter. The predicted vs. actual plot implies that both responses show a great fit between predicted and actual values.

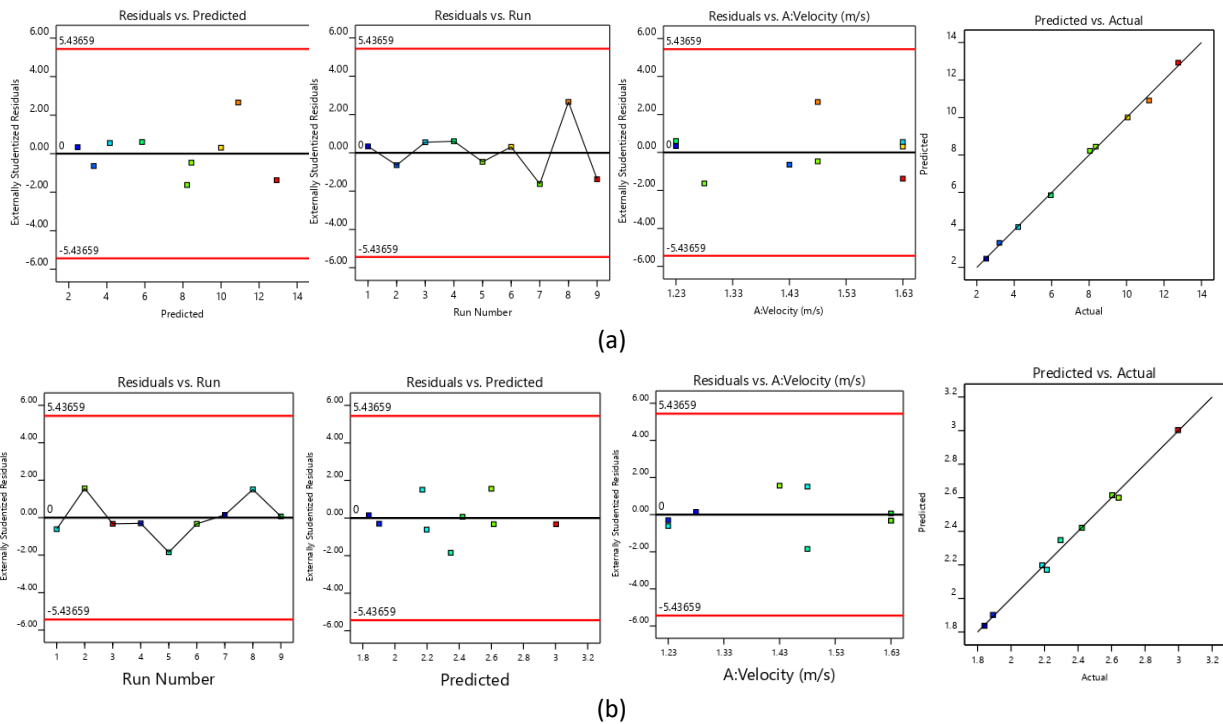


Fig. 5. Diagnostics of residuals, predicted, run, and actual of (a) voltage and (b) pressure drop

The model graph evaluates how both factors interact with the response. The perturbation plot compares the effects of all factors at a specific point. The response is plotted while holding other factor constants. The slope indicates how sensitive the response is to the corresponding factor. For voltage in Figure 6(a), magnetic field strength shows higher sensitivity compared to velocity. Meanwhile, velocity shows great sensitivity to the response in pressure drops, while magnetic field strength shows the same tendency but with an inverse effect. The factor of interaction AB of the black line in Figure 6(b) represents the lower limit, while the red line represents the upper limit. When it comes to voltage, the higher limit is located above the lower limit, while it is the opposite for pressure drop. This suggests that the voltage rises as factor interaction does; on the other hand, the pressure drop will decrease. This outcome is consistent with the regression equation covered in the previous section.

Contour and 3D surface graphs plot both factors in the x and y -axis, while the corresponding response as a dependent variable on the z -axis is visualized in Figure 7 and 8. The colour indicates the range of responses for easier analysis. On the 3D surface in Figure 8, the plot in the form of a sloping plane shows the model of two-factor interaction between factors for each response. Figures 7(a) and 8(a) plotted the voltage response, whose objective is to be maximized, so the desired area is located at the top right in the red shade. The pressure drop response, plotted in Figures 7(b) and 8(b), aims to be minimized; hence, the desired area is located at the top left in the blue shade.

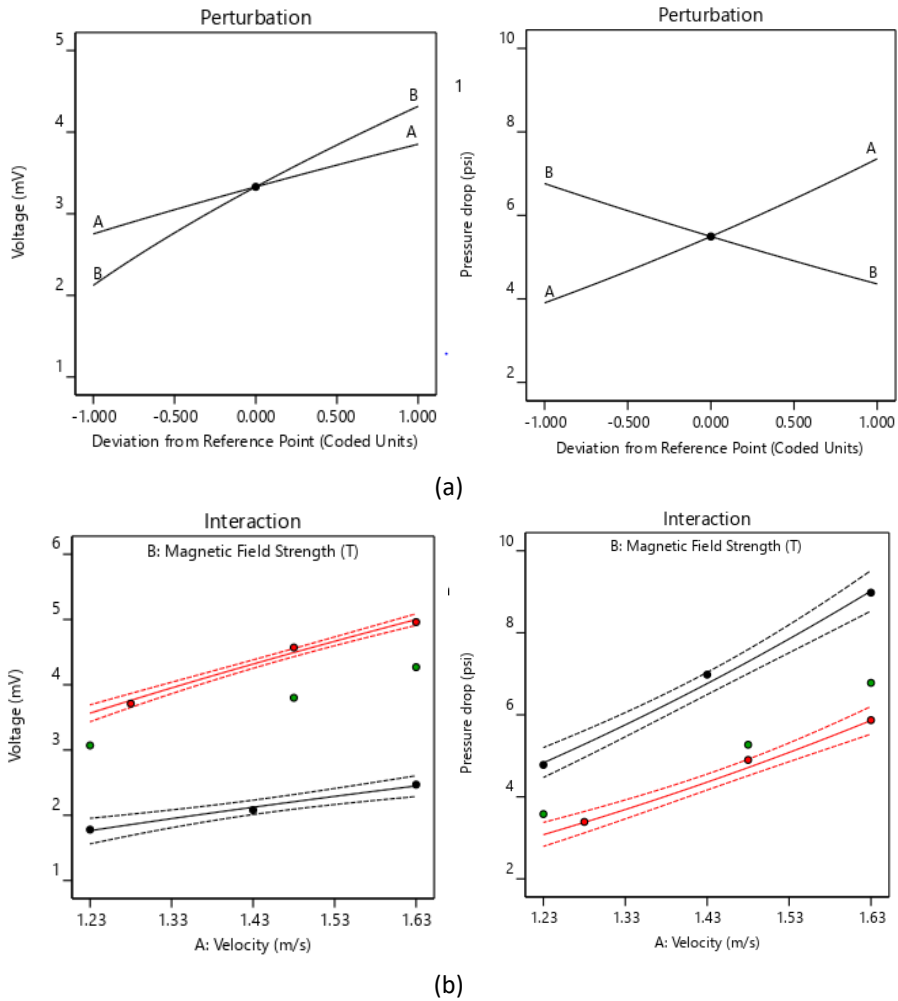


Fig. 6. Model graph for (a) perturbation and (b) factor interaction of voltage and pressure drop

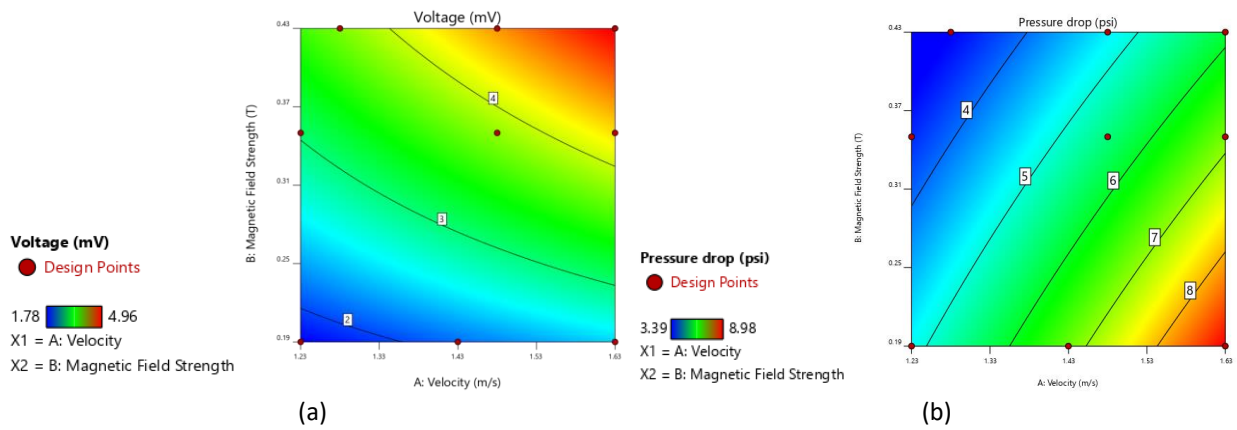


Fig. 7. 3D Surface of (a) voltage and (b) pressure drop

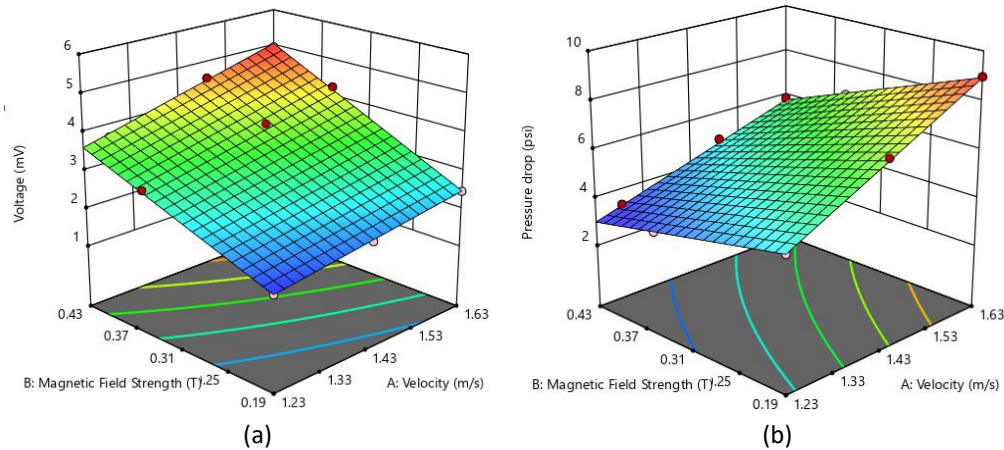


Fig. 8. Contour of (a) voltage and (b) pressure drop

Several measurements were used to compare both models. R^2 measures the predictive model's performance, while RMSE measures the error or difference between the predictive and actual values. RSM estimated R^2 to be close to one, implying that the models developed by RSM are effective at predicting responses. The result of RSM predictive modelling is implied in Table 4. Both responses, voltage and pressure drop indicate that the data's nature is less complex and can be described by two input parameters and two responses. The regression function precisely describes the simplicity with a high R^2 value and very low RMSE.

Table 4

RSM performance parameter

Response	Voltage	Pressure drops
R^2	0.9983	0.9939
RMSE	0.142	0.027
Optimum value	3.303 mV	2.7 psi

3.2 RSM Optimization

Once the mathematical model is established, optimization techniques are applied to identify the optimal conditions for the system. The goal is to find the combination of input factors that maximizes or minimizes the desired responses. Numerical optimization was performed within the same software by defining the boundary range of all parameters. The range shown in Figure 9 was performed in full range due to limited data. After trial-and-error, it also shows this range provides an excellent desirability rating in the solutions.

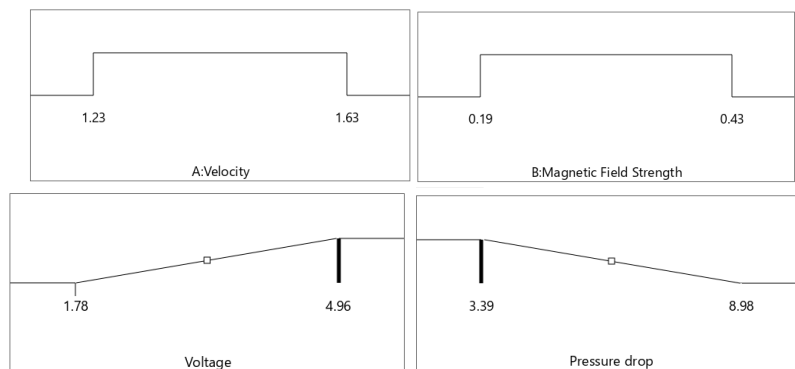


Fig. 9. Numerical criteria for RSM optimization

Additionally, the weight is set to be the same for all parameters, indicating that the factors and answers have the same degree of importance. The weight is 1, the importance value is 3, and the optimization constraints are shown in Table 5.

Table 5
 Constraints of RSM optimization

Variables	Goal	Lower limit	Upper limit
Velocity	Is in range	1.23	1.63
Magnetic field strength	Is in range	0.19	0.43
Voltage	Maximize	1.78	4.96
Pressure drops	Minimize	3.39	8.98

The number of solutions and the solutions as a result of optimization were also compared. Recall the objective of maximizing voltage and minimizing pressure drop. The desirability algorithm works based on mathematical functions that quantify how they align the actual value within predefined target ranges. The desirability value reflects the closeness of the actual response value to the target value or range. A desirability value of 1 means the response is precisely at the target, while a value closer to 0 indicates a larger deviation from the target. With the boundary setup, RSM numerical optimization derives 11 possible solutions with desirability as a measurement of the optimization performance. The higher the desirability, the more optimal the solution. Desirability in Table 6 ranges from 0.768 to 0.770, and the value between each alternative solution does not have a significant discrepancy. As per suggestion, option number 1 is selected as the most optimal solution. It is selected with a velocity of 1.415 m/s and magnetic field strength of 0.43 T, resulting in a response of voltage of 4.264 mV and pressure drop of 4.254 psi. This solution is based on the predictive-based model using a regression equation.

Table 6
 Solutions of RSM optimization

No.	Factors		Responses		Desirability
	A: Velocity (m/s)	B: Magnetic field strength (T)	Voltage (mV)	Pressure drops (psi)	
1	1.415	0.430	4.264	4.254	0.770
2	1.417	0.430	4.271	4.267	0.770
3	1.413	0.430	4.256	4.238	0.770
4	1.421	0.430	4.284	4.292	0.770
5	1.407	0.430	4.235	4.199	0.770
6	1.423	0.430	4.294	4.312	0.770
7	1.402	0.430	4.216	4.163	0.770
8	1.397	0.430	4.198	4.130	0.770
9	1.386	0.430	4.157	4.054	0.769
10	1.375	0.430	4.118	3.982	0.768
11	1.367	0.430	4.088	3.928	0.768

The generated solutions relation with both variables are visualized in Figure 10. High desirability is preferred, so the area of selected solutions is in the middle-top, showing that high performance is obtained with about the middle value of velocity range and high magnetic field strength, which can be seen in Figure 10(a). Trade-off of both responses is shown by a reversed contour in pressure drop, the specifically variable magnetic field strength in Figure 10(c), while in voltage in Figure 10(b), the desired area is located in the corner of the right top.

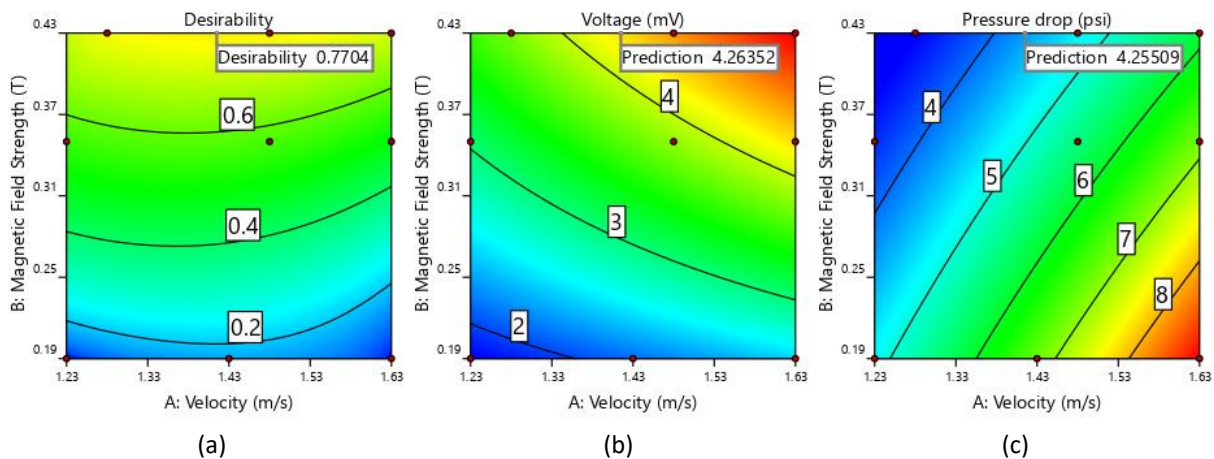


Fig. 10. Contour of Response Surface Methodology (RSM) solutions (a) desirability, (b) voltage, and (c) pressure drop

By specifically exploring the optimal operating parameters of fluid velocity and magnetic field strength, our study not only enhances the scientific understanding but also offers practical insights crucial for developing highly efficient energy conversion systems. This knowledge has direct relevance to real-world scenarios, potentially leading to the design and implementation of MHD generators that can significantly improve energy conversion efficiency and contribute to sustainable energy practices.

4. Conclusions

In this study, we employed Response Surface Methodology (RSM) for modelling and optimizing a vortex MHD generator using mercury as the working fluid. The secondary dataset comprised 9 data points, with two input factors (velocity and magnetic field strength) and two responses (voltage and pressure drop), targeted for maximization and minimization, respectively. Given the limited dataset with only two inputs and two responses, the statistical approach of RSM was deemed appropriate.

To model and predict data, RSM utilizes mathematical formulations based on independent and dependent variables. Our results, evaluated through R^2 and RMSE, consistently demonstrated the effectiveness of the RSM method. The high R^2 values for voltage (0.9982) and pressure drop (0.9939) indicated a robust representation of observed data. Additionally, the RMSE values for voltage (0.142) and pressure drop (0.027) were within acceptable limits, affirming the model's high predictive accuracy.

To identify optimal responses, we generated a total of 11 solutions. The RSM method proposed that applying a velocity of 1.415 m/s and a magnetic field strength of 0.43 T would yield a voltage of 4.264 mV and a pressure drop of 4.254 psi. The desirability measurement for this selected solution was calculated as 0.770.

In summary, our research employed RSM successfully, demonstrating its applicability to the specific case of a vortex MHD generator with mercury as the working fluid. The results highlight the model's accuracy and efficiency in optimizing the system's performance. For upcoming works, the generation of data by validation experiments will enhance the robustness of the current optimization study, and randomization trials must be performed as well. Subsequently, more data increases accuracy by opening up the possibility to alternative techniques like artificial neural networks (ANN). Future research will take into account more input factors and optimization issues such as minimizing energy losses.

Acknowledgement

The financial support from RISBANG Universitas Indonesia through the PUTI Q3 2020 contract number NKB-2009/UN2.RST/HKP.05.00/2020 is truly acknowledged.

References

- [1] Sheikholeslami, M., Z. Khalili, P. Scardi, and N. Ataollahi. "Environmental and energy assessment of photovoltaic-thermal system combined with a reflector supported by nanofluid filter and a sustainable thermoelectric generator." *Journal of Cleaner Production* 438 (2024): 140659. <https://doi.org/10.1016/j.jclepro.2024.140659>
- [2] Sheikholeslami, M., and Z. Khalili. "Environmental and energy analysis for photovoltaic-thermoelectric solar unit in existence of nanofluid cooling reporting CO2 emission reduction." *Journal of the Taiwan Institute of Chemical Engineers* 156 (2024): 105341. <https://doi.org/10.1016/j.jtice.2023.105341>
- [3] Takeda, Minoru, Yasuaki Okuji, Teruhiko Akazawa, Xiaojun Liu, and Tsukasa Kiyoshi. "Fundamental studies of helical-type seawater MHD generation system." *IEEE transactions on applied superconductivity* 15, no. 2 (2005): 2170-2173. <https://doi.org/10.1109/TASC.2005.849604>
- [4] Ryan, Drew, Corey Loescher, Ian Hamilton, Robert Bean, and Adam Dix. "Magnetic variation and power density of gravity driven liquid metal magnetohydrodynamic generators." *Annals of Nuclear Energy* 114 (2018): 325-328. <https://doi.org/10.1016/j.anucene.2017.12.047>
- [5] Kobayashi, Hiromichi, Hiroki Shionoya, and Yoshihiro Okuno. "Turbulent duct flows in a liquid metal magnetohydrodynamic power generator." *Journal of Fluid Mechanics* 713 (2012): 243-270. <https://doi.org/10.1017/jfm.2012.456>
- [6] Cosoroaba, Eva, Carlos Caicedo, Lizon Maharjan, Adam Clark, Minxiang Wu, Jingchen Liang, Mehdi Moallem, and Babak Fahimi. "3D multiphysics simulation and analysis of a low temperature liquid metal magnetohydrodynamic power generator prototype." *Sustainable Energy Technologies and Assessments* 35 (2019): 180-188. <https://doi.org/10.1016/j.seta.2019.05.012>
- [7] Tang, Lu, Baolin Liu, Qi Xia, and Aiwu Peng. "Three-Dimensional Analysis of the Influence of the Magnetic Flux Density on Minimum PR in a Faraday-Type MHD Channel." *IEEE Transactions on Plasma Science* 50, no. 2 (2022): 417-424. <https://doi.org/10.1109/TPS.2021.3139432>
- [8] Zhu, Shunmin, Tong Wang, Chao Jiang, Zhanghua Wu, Guoyao Yu, Jianying Hu, Christos N. Markides, and Ercang Luo. "Experimental and numerical study of a liquid metal magnetohydrodynamic generator for thermoacoustic power generation." *Applied Energy* 348 (2023): 121453. <https://doi.org/10.1016/j.apenergy.2023.121453>
- [9] Li, Lai, Hu-lin Huang, and Gui-ping Zhu. "Numerical Simulations for a Partial Disk MHD Generator Performance." *Energies* 11, no. 1 (2018): 127. <https://doi.org/10.3390/en11010127>
- [10] Domínguez-Lozoya, José Carlos, Sergio Cuevas, David Roberto Domínguez, Raúl Ávalos-Zúñiga, and Eduardo Ramos. "Laboratory characterization of a liquid metal MHD generator for ocean wave energy conversion." *Sustainability* 13, no. 9 (2021): 4641. <https://doi.org/10.3390/su13094641>
- [11] Orozco, Juan Adrián Pérez, and Raúl Alejandro Avalos Zúñiga. "Theoretical model of a DC magnetohydrodynamic generator in annular geometry." *INGENIERÍA MECÁNICA TECNOLOGÍA Y DESARROLLO* 6, no. 6 (2020): 227-234.
- [12] Fouad, A. A., and H. J. Weiss. "End losses in a magnetohydrodynamic channel: Dc channel with fluid having large magnetic Reynolds number." *IEEE Transactions on Electron Devices* 7 (1966): 554-561. <https://doi.org/10.1109/T-ED.1966.15734>
- [13] Ávalos-Zúñiga, Raúl A., and Michel Rivero. "Theoretical modeling of a vortex-type liquid metal MHD generator for energy harvesting applications." *Sustainable Energy Technologies and Assessments* 52 (2022): 102056. <https://doi.org/10.1016/j.seta.2022.102056>
- [14] West, Devin, J. Ashley Taylor, and Tom Krupenkin. "Alternating current liquid metal vortex magnetohydrodynamic generator." *Energy Conversion and Management* 223 (2020): 113223. <https://doi.org/10.1016/j.enconman.2020.113223>
- [15] Panchadar, Karan, Devin West, J. Ashley Taylor, and Tom Krupenkin. "Mechanical energy harvesting using a liquid metal vortex magnetohydrodynamic generator." *Applied Physics Letters* 114, no. 9 (2019). <https://doi.org/10.1063/1.5078384>
- [16] Gupta, Siddharth Raj, J. Ashley Taylor, and Tom Krupenkin. "Three-phase alternating current liquid metal vortex magnetohydrodynamic generator." *Iscience* 24, no. 6 (2021). <https://doi.org/10.1016/j.isci.2021.102644>
- [17] Gupta, Siddharth Raj, J. Ashley Taylor, and Tom Krupenkin. "Theoretical investigation of a novel three-phase alternating current liquid metal vortex magnetohydrodynamic generator." *Sustainable Energy Technologies and Assessments* 53 (2022): 102436. <https://doi.org/10.1016/j.seta.2022.102436>

- [18] Jalili, Bahram, Ali Mirzagoli Ganji, Amirali Shateri, Payam Jalili, and Davood Domiri Ganji. "Thermal analysis of Non-Newtonian visco-inelastic fluid MHD flow between rotating disks." *Case Studies in Thermal Engineering* 49 (2023): 103333. <https://doi.org/10.1016/j.csite.2023.103333>
- [19] Jalili, Payam, Ali Ahmadi Azar, Bahram Jalili, and Davood Domiri Ganji. "The HAN method for a thermal analysis of forced non-Newtonian MHD Reiner-Rivlin viscoelastic fluid motion between two disks." *Heliyon* (2023). <https://doi.org/10.1016/j.heliyon.2023.e17535>
- [20] Ray, Sourav, Mohaiminul Haque, Tanvir Ahmed, and Taifa Tasnim Nahin. "Comparison of artificial neural network (ANN) and response surface methodology (RSM) in predicting the compressive and splitting tensile strength of concrete prepared with glass waste and tin (Sn) can fiber." *Journal of king saud university-engineering sciences* 35, no. 3 (2023): 185-199. <https://doi.org/10.1016/j.jksues.2021.03.006>
- [21] Zhu, Jun, Shaolong Li, Dandan Song, Qiaoli Han, Jingmei Wang, and Guanghua Li. "Multi-objective optimisation design of air-cored axial flux PM generator." *IET Electric Power Applications* 12, no. 9 (2018): 1390-1395. <https://doi.org/10.1049/iet-epa.2018.5092>
- [22] Sunarti, A. R., and A. L. Ahmad. "Performances of Automated Control System for Membrane Gas Absorption: Optimization Study." *Journal of Advanced Research in Applied Mechanics* 6 (2015): 1-20.
- [23] Narwade, P. A., and Supriya R. Deshmukh. "An RSM approach to maximize fundamental frequency of e-glass epoxy composite panels." *Journal of Advanced Research in Applied Mechanics* 35, no. 1 (2017).
- [24] Kong, Chuang, Meng Wang, Tao Jin, and Shaoliang Liu. "The blade shape optimization of a low-pressure axial fan using the surrogate-based multi-objective optimization method." *Journal of Mechanical Science and Technology* 37, no. 1 (2023): 179-189. <https://doi.org/10.1007/s12206-022-1219-y>
- [25] Kim, Beom Seok, Bong Seop Kwak, Sangwoo Shin, Sanghoon Lee, Kyung Min Kim, Hyo-Il Jung, and Hyung Hee Cho. "Optimization of microscale vortex generators in a microchannel using advanced response surface method." *International journal of heat and mass transfer* 54, no. 1-3 (2011): 118-125. <https://doi.org/10.1016/j.ijheatmasstransfer.2010.09.061>
- [26] Salviano, Leandro O., Daniel J. Dezan, and Jurandir I. Yanagihara. "Optimization of winglet-type vortex generator positions and angles in plate-fin compact heat exchanger: response surface methodology and direct optimization." *International Journal of Heat and Mass Transfer* 82 (2015): 373-387. <https://doi.org/10.1016/j.ijheatmasstransfer.2014.10.072>
- [27] Liu, Zhenwei, Cameron McGregor, Songlin Ding, and Xu Wang. "Study of a three-dimensional model simulation of a speed amplified flux switching linear generator for wave energy conversion and its design optimization in the ocean environment." *Energy* 284 (2023): 128625. <https://doi.org/10.1016/j.energy.2023.128625>
- [28] Si, Jikai, Zuoguang Yan, Rui Nie, Zhongwen Li, Yihua Hu, and Yingsheng Li. "Multi-objective optimization of a tubular permanent magnet linear generator with 120° phase belt toroidal windings using response surface method and genetic algorithm." *IET Renewable Power Generation* 16, no. 2 (2022): 352-361. <https://doi.org/10.1049/rpg2.12328>
- [29] Lee, Sung-Ho, Yong-Jae Kim, Kyu-Seok Lee, and Sung-Jin Kim. "Multiobjective optimization design of small-scale wind power generator with outer rotor based on Box-Behnken design." *IEEE Transactions on Applied Superconductivity* 26, no. 4 (2016): 1-5. <https://doi.org/10.1109/TASC.2016.2524620>
- [30] Ibáñez, Guillermo, Sergio Cuevas, and Mariano López de Haro. "Optimization analysis of an alternate magnetohydrodynamic generator." *Energy Conversion and Management* 43, no. 14 (2002): 1757-1771. [https://doi.org/10.1016/S0196-8904\(01\)00133-9](https://doi.org/10.1016/S0196-8904(01)00133-9)
- [31] Carcangiu, Sara, Alessandra Fanni, and Augusto Montisci. "Optimal Design of an Inductive MHD Electric Generator." *Sustainability* 14, no. 24 (2022): 16457. <https://doi.org/10.3390/su142416457>
- [32] Atmanlı, Alpaslan, Bedri Yüksel, Erol Ileri, and A. Deniz Karaoglan. "Response surface methodology based optimization of diesel-n-butanol-cotton oil ternary blend ratios to improve engine performance and exhaust emission characteristics." *Energy Conversion and Management* 90 (2015): 383-394. <https://doi.org/10.1016/j.enconman.2014.11.029>
- [33] Naveen, N. Raghavendra, Mallesh Kurakula, and Buduru Gowthami. "Process optimization by response surface methodology for preparation and evaluation of methotrexate loaded chitosan nanoparticles." *Materials Today: Proceedings* 33 (2020): 2716-2724. <https://doi.org/10.1016/j.matpr.2020.01.491>